Journal of Computer-Aided Molecular Design, **13:** 385–396, 1999.
KLUWER/ESCOM

Conformational variety for the ansa chain of rifamycins: Comparison of observed crystal structures and molecular dynamics simulations

Alessia Bacchi* & Giancarlo Pelizzi
Dipartimento di Chimica Generale ed Inorganica, Chimica Analitica, Chimica Fisica, Università di Parma, Viale delle Scienze, I-43100 Parma, Italy

Received 7 April 1998; Accepted 13 November 1998

Key words: Cambridge Crystallographic Database, circular statistics, structure correlation, torsion angles

Summary

The antibiotic activity (via inhibition of DNA-dependent RNA polymerase, DDRP) of rifamycins has been correlated to the conformation of the ansa chain, which can be described by means of 17 torsion angles defined along the ansa backbone. It has been shown that favourable or unfavourable conformations of the ansa chain in rifamycin crystals are generally diagnostic of activity or inactivity against isolated DDRP. The principles of structure correlation suggest that the torsional variety observed in rifamycin crystals should mimic the dynamic flexibility of the ansa chain in solution. Twenty-six crystal structures of rifamycins are grouped into two classes (active and non-active). For each class the variance of the 17 ansa backbone torsion angles is analysed. Active compounds show a well-defined common pattern, while non-active molecules are more scattered, mainly due to steric constraints forcing the molecules into unfavourable conformations. The experimental distributions of torsion angles are compared to the torsional freedom of the ansa chain simulated by molecular dynamics calculations performed at different temperatures and conditions on rifamycin S and rifamycin O, which represent a typical active and a typical sterically constrained molecule, respectively. It is shown that the torsional variety found in the crystalline state samples the dynamic behaviour of the ansa chain for active compounds. The methods of circular statistics are illustrated to describe torsion angle distributions.

Introduction

Rifamycins are naphthalenic ansamycins made by a naphthoquinonic system, either in the oxidated or in the reduced form, condensed to a furanone ring (chromophore) spanned by a 17-membered ansa chain connecting two opposite sides of the chromophore. Several rifamycin derivatives are known, generally differing in the substitution at positions 3 and 4 of the chromophore. Two of these, rifamycin S and rifamycin O, are shown in Scheme 1, along with their three-dimensional structure.

Rifamycins exert their antibiotic activity by specific inhibition of bacterial DNA-dependent RNA polymerase (DDRP). They exhibit activity against a variety of organisms, such as bacteria, eukaryotes and viruses, and for this reason they are sometimes called 'wonder drugs' [1]. A number of rifamycin derivatives have been studied during the last 30 years. The mode of enzymatic inhibition is not known since neither the structure of the complex between rifamycin and DDRP, nor of isolated DDRP, have ever been determined. In the absence of first-hand information, several studies have related the solid-state structure of active rifamycins to the conditions needed for activity [2–9]. Scheme 2 shows the qualitative model that has been developed and is generally accepted [1,5] to explain the mechanism of action of rifamycins. It involves the formation of hydrogen bonds between the enzyme and four rifamycin oxygens (O1, O2, O9, O10), which must be arranged in a specific favourable three-dimensional pattern. The crystal structures of ri-

*To whom correspondence should be addressed.
E-mail: bacchi@ipruniv.cce.unipr.it

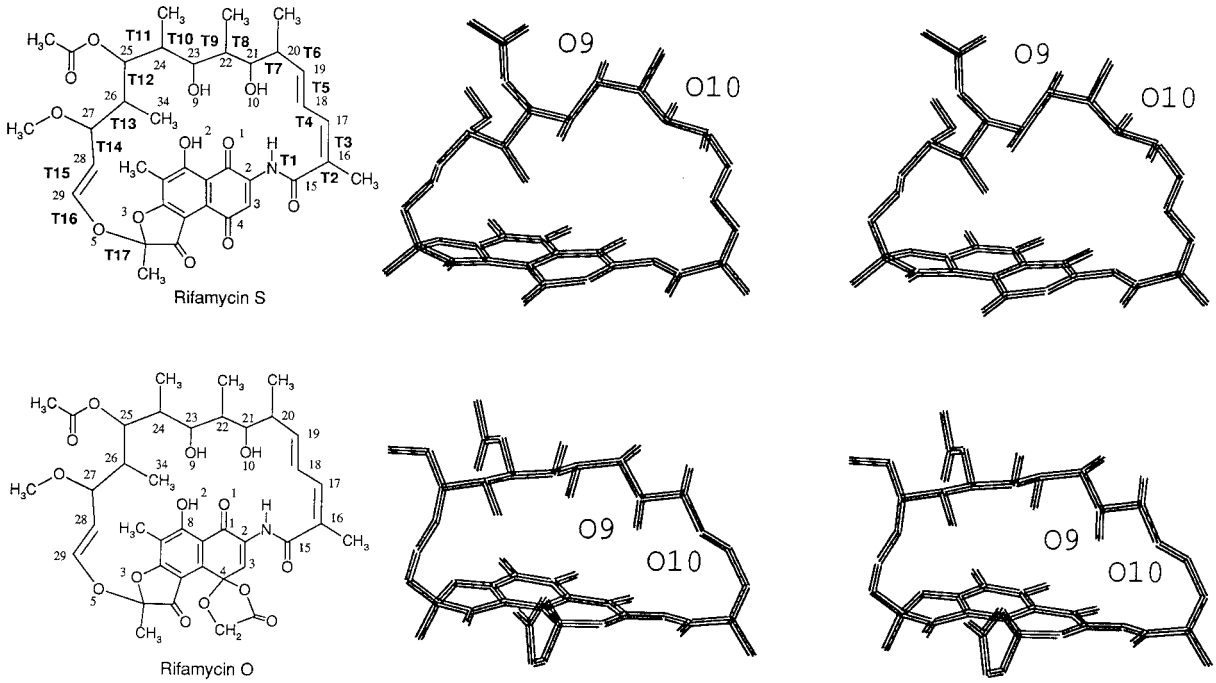

Scheme 1. Molecular schemes and stereoview of the crystal structures for rifamycin S [20] (top) and rifamycin O [9] (bottom). Torsion angles used in the analysis are indicated for rifamycin S along with relevant atomic numbering.

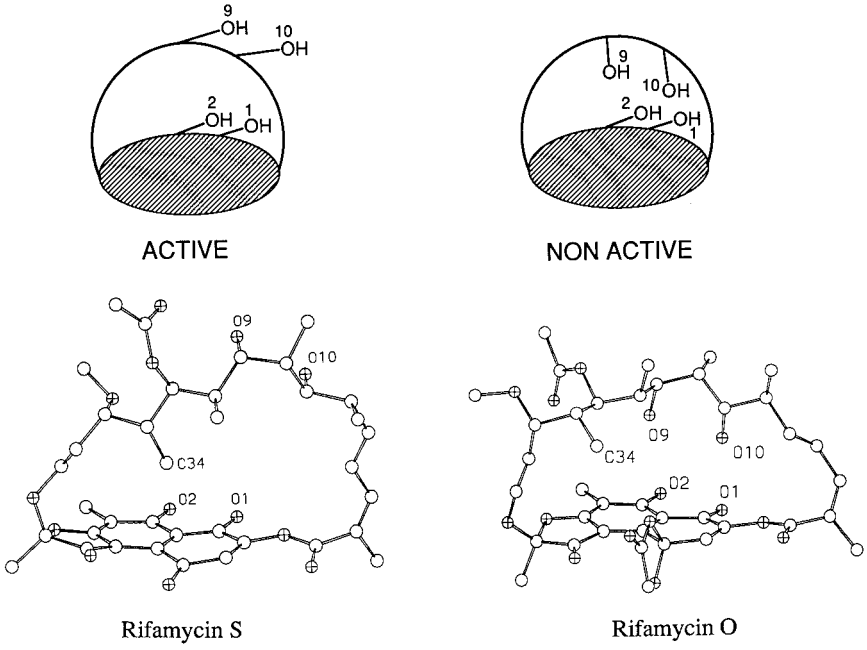

Scheme 2. Top: Qualitative model of structural requirements for activity, showing that bonds C21-O10 and C23-O9 must be approximately parallel to the chromophore. Bottom: Crystal structures of rifamycin S and rifamycin O. Heteroatoms are indicated with shaded circles. In rifamycin S, the ansa mean plane is approximately perpendicular to the naphthoquinone. O1, O2, O9 and O10 point out of the same side of the molecule and C34 is oriented towards the chromophore. In rifamycin O, methyl C34 is hindered by the oxolanone 4-substituent and O9 and O10 point towards the chromophore.

famycin S and rifamycin O are also shown to illustrate the structural features of the model.

The quantitative characterisation of this pattern has been provided by performing multivariate statistical analysis on geometric parameters derived from rifamycin crystal structures [8–10]. It has been shown [9] that the geometric arrangement of the pharmacophore (O1, O2, O9, O10) is determined by the conformation of the ansa chain, which can be described by 17 torsion angles involving the bonds along the ansa backbone, as defined in Scheme 1. In particular, on the basis of crystal data and conformational analysis performed by molecular mechanics, two factors affecting the pharmacophore geometry have been described. The first involves a rotation of the central section of the ansa chain (C19-C28) around the bonds C19-C20 and C26-C27. The second factor is related to local conformational rearrangements in the vicinity of the atoms carrying O9 and O10, namely between C20 and C24. In this work, we compare the information retrievable by analysing the distribution of conformations observed in rifamycin crystal structures with the results of molecular dynamics simulations carried out on two rifamycin molecules, rifamycin S and rifamycin O, representative of active and non-active compounds, respectively, as shown in Scheme 2. This comparative analysis may help to determine which are the most flexible locations in the molecule, and to understand whether reasonable mechanisms exist which can convert the conformations observed in the solid state into significantly different conformers.

Materials and methods

Crystallographic data

The Cambridge Structural Database [11] facilities at the Centro di Studio per la Strutturistica Diffrattometrica in Parma were used to retrieve structural data for all rifamycins characterised by X-ray diffraction [2–8, 12–22]. In some cases [6,15], coordinates were not deposited and were kindly provided by the authors. In the course of the analysis, we found that three rifamycins (five independent molecules) appear in the literature and in the Cambridge Structural Database with the wrong absolute configuration, seriously affecting the discussions based on torsion angles. In the present work, all values have been revised and fixed.

Molecular dynamics simulations

Molecular dynamics simulations were performed on rifamycin S [20] and rifamycin O [9], by using the observed crystal structures as the starting conformation. Hydrogen geometries were renormalised and the intramolecular hydrogen bonds O1-H···O2 and O10-H···O9 were preserved. Calculations were performed with the program SYBYL [23], using the standard Tripos force-field. Since intramolecular hydrogen bonds are likely to play an important role in determining the energy of conformational rearrangements, particular care was taken in choosing a suitable description of partial charge distribution on atoms. Atomic charges were derived from the electrostatic potential calculated by performing a single-point ab initio calculation with the STO-3G basis set on the experimental molecular structures with Gaussian92 [24]. A 16 Å cut-off was used for including electrostatic contributions in the dynamic simulation. The properties of the force-field, atomic charges, dielectric constant value, were chosen to be consistent with the molecular mechanics calculations reported for the torsional rearrangement, in vacuo, of torsion angles T4, T6 and T13 for rifamycin S and rifamycin O [9]. The simulations were performed for 80 ps. The equilibration of the system was attained during the initial 1000 fs, which were discarded from the following analysis. Atomic coordinates were stored every 50 fs. Different conditions were tested: (a) $T = 300$ K, in vacuo, $\epsilon = 1.5$; (b) $T = 370$ K, in vacuo, $\epsilon = 1.5$; (c) $T = 300$ K, in vacuo, the effect of solvent was simulated by including distance dependence for ϵ, as implemented in SYBYL. Run c was extended to 1000 ps (run d) to check whether any additional low-frequency conformational conversion could appear.

Methods for circular statistics analysis

In linear statistics, the mean (m) and standard deviation (s) of a sample of N data $x(i)$ are defined as

$$m = \frac{1}{N}\sum_{1}^{N} x(i)$$

and

$$s = \sqrt{\frac{1}{N}\sum_{1}^{N}[x(i) - m]^2}$$

Torsion angles are periodic variables conventionally defined between $-180°$ and $180°$. As pointed out by

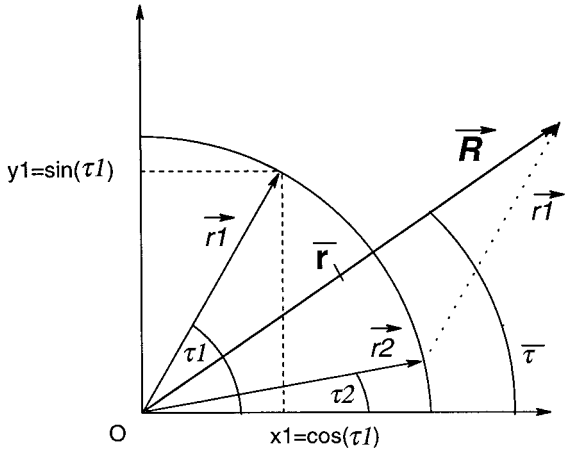

Scheme 3. Determination of the circular mean of two torsion angles: τ1 and τ2 (here both in the first quadrant for simplicity) are reported on the unit circle to build the unit vectors $\vec{r}1$ and $\vec{r}2$. The resultant vector $\vec{R} = \vec{r}1 + \vec{r}2$ defines the mean direction $\overline{\tau}$. The concentration parameter $\bar{r}$ is obtained by dividing the length of $\vec{R}$ by $N = 2$.

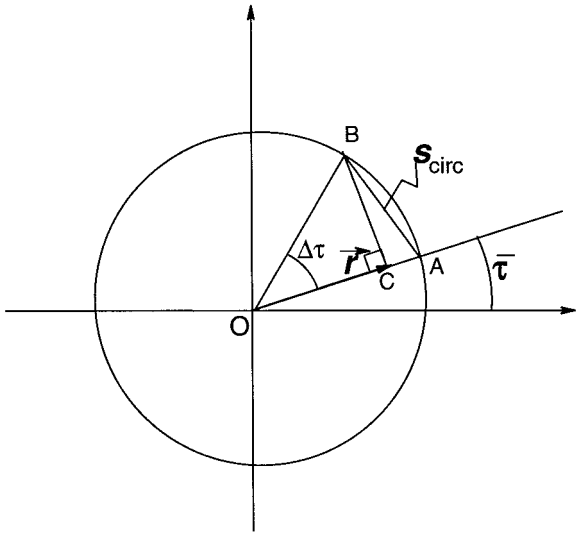

Scheme 4. Given the direction of the mean vector, *OA*, the perpendicular is drawn from the extremity *C* of the concentration parameter vector $\vec{r}$. *B* is the intersection of the perpendicular with the unit circle. The chord $\overline{AB}$ (expressed in radians) represents s_{circ}. The angle $\Delta\tau$ corresponds to the chord $\overline{AB}$ and to the arc $\widehat{AB}$.

Allen and Johnson [25], if linear statistics are applied to torsion angles, misleading results can be obtained. For instance, for $x(1) = +179°$ and $x(2) = -179°$ one would obtain $m = 0°$, $s = 253°$, while in fact both values are very close to 180°, spanning a range of only 2°. The tools of circular statistics [26] are appropriate to describe distributions of torsion angles $\tau(i)$, which can be associated to unit vectors $\vec{r}(i)$ in the xy plane, with components $x(i) = \cos\tau(i)$ and $y(i) = \sin\tau(i)$ (Scheme 3).

The circular mean $\overline{\tau}$ is defined as the direction of the vector $\vec{R}$ resultant from the sum of the unit vectors $\vec{r}(i)$ corresponding to the N torsion angles:

$$\overline{\tau} = \tan^{-1}\left[\frac{\sum_1^N \sin\tau(i)}{\sum_1^N \cos\tau(i)}\right]$$

The length of $\vec{R}$ is a measure of the concentration of single vectors about the mean direction. The length of the mean vector $|\boldsymbol{R}|/N = \bar{r}$ is called the *concentration parameter* and ranges from 0 (no preferred direction) to 1 (all vectors are parallel).

$$\bar{r} = \frac{1}{N}\sqrt{\left(\sum_1^N \sin\tau(i)\right)^2 + \left(\sum_1^N \cos\tau(i)\right)^2}$$

The relations $\sum_1^N \sin(\tau(i) - \overline{\tau}) = 0$ and $\sum_1^N \cos(\tau(i) - \overline{\tau}) = N\bar{r}$ hold.

The dispersion of $\tau(i)$ around the mean is related to $\bar{r}$. Various methods have been reported to derive an expression for the circular standard deviation s_{circ} [25–27]. We chose to follow Batschelet's method [26], which has the advantage over other approaches that s_{circ} does not diverge for small values of $\bar{r}$.

$$s_{\text{circ}} = \sqrt{2(1-\bar{r})} \text{ (in radians)}$$

It follows that

$$s_{\text{circ}}^2 = \frac{1}{N}\sum_1^N 2\,[1 - \cos(\tau(i) - \overline{\tau})]$$

The geometric meaning of s_{circ} is shown in Scheme 4.

For small angular deviations $[\tau(i) \approx \overline{\tau}]$, the properties

$$\sin(\tau(i) - \overline{\tau}) \approx (\tau(i) - \overline{\tau}) \tag{1a}$$

and

$$\cos(\tau(i) - \overline{\tau}) \approx 1 - \frac{1}{2}(\tau(i) - \overline{\tau})^2 \tag{1b}$$

are known. Accordingly, Batschelet has shown that for distributions with small dispersion the circular mean and standard deviations converge to the corresponding linear expressions. Relations 1 may be used to evaluate

the extent to which it is appropriate, in first approximation, to use linear statistics in the description of circular data. Given the arc $(\tau(i) - \overline{\tau} = \Delta\tau)$ on the unit circle (see for instance the arc $\widehat{AB}$ in Scheme 4), the length of the chord $\overline{AB}$ is $\sqrt{2[1 - \cos(\tau(i) - \overline{\tau})]}$. Expressions 1 are valid when $\widehat{AB} \approx \overline{AB}$. For $(\tau(i) - \overline{\tau}) = 0.5$ rad (30°), the systematic discrepancy between linear and circular methods associated with the use of relations 1 is about 1% in radii length units, and it grows to 5% for an angular spread of 60°.

Circular means have been used to calculate the correlation coefficient (*corr*) between torsion angles:

$$corr(k,l) = \frac{\sum_1^N [\tau(i,k) - \overline{\tau}(k)][\tau(i,l) - \overline{\tau}(l)]}{\sqrt{\sum_1^N [\tau(i,k) - \overline{\tau}(k)]^2 \sum_1^N [\tau(i,l) - \overline{\tau}(l)]^2}}$$

In computing *corr*(*k*,*l*) the angle with the smallest absolute value between $[\tau(i, j) - \overline{\tau}(j)]$ and its supplement must be considered. For instance, the difference between +100° and −100° should be −160° and not +200°. The significance of *corr*(*k*,*l*) has been assessed as the complement to 1 of the probability $p(|corr|, N)$ that a random sample of N uncorrelated data points would give a correlation coefficient greater than or equal to $|corr|$ [28].

$$p(|corr|, N) = \frac{2}{\sqrt{\pi}} \frac{\Gamma\left[(\nu+1)/2\right]}{\Gamma\left[\nu/2\right]} \int_{|corr|}^{1} \left(1 - x^2\right)^{(\nu-2)/2} \mathrm{d}x$$

where $\nu = N - 2$ and Γ is the gamma function.

Results

The Cambridge Structural Database [11] was searched to retrieve structural data for all rifamycins characterised by X-ray diffraction [2–8,12–22]. To these, data concerning rifamycin O were added [9], for a total of 26 independent molecules, comprising chemically different derivatives, different polymorphs, and different symmetry independent molecules present in the same crystal. They were grouped into two classes: active (16) and non-active (10) compounds, according to activity data reported in the original literature*.

*List of compounds considered. Some of them appear in more than one crystalline form. a = active, n.a. = non-active. Rifamycin S (a), rifamycin S iminomethyl ether (n.a.), cyclised rifamycin SV (n.a.), tolypomycinone (n.a.), 3-methoxycarbonyl rifamycin S (a), sodium rifamycin SV (a), 21-acetoxy-11(*R*)-rifamycinol S (n.a.), rifamycin B (a), rifamycin Y (n.a.), 25-*O*-deacetyl-27,28-didehydro-27-demethoxy-11-deoxo-11,29-epoxy-28,29-dihydro-21,23-*O*-isopropylidene rifamycin S (n.a.), rifamycin L105 (a), rifamycinol S (a), (11*R*)-25-*O*-deacetyl-11-deoxo-11-hydroxy-21,23-*O*-isopropylidene rifamycin S (n.a.), rifamycin P (a), rifampicine (a), (16*S*)-16,17,18,19-tetrahydro rifamycin S (a), rifamexil (a), rifamycin O (a, see the Discussion section).

Torsion angles from T1 to T17 (see Scheme 1 for the definition) were calculated for each molecule and the relative distribution of values was characterised by circular statistics, taking into account the periodic nature of the variables [25,26]. Figures 1a and b show the distribution of torsion angles along the ansa chain backbone for active and non-active rifamycins, respectively, whereas Table 1 reports the summary circular statistics for the two distributions.

The analogies between torsional variety observed in the solid state and conformational flexibility have been investigated by performing molecular dynamics simulations for rifamycin S and rifamycin O, as examples of active and non-active molecules.

In Figures 1a and b, the ansa chain torsion angles relative to the starting conformations for the two molecules are highlighted. Figures 2, 3 and 4 report the torsion angle distributions obtained by the molecular ensembles stored for runs a (T = 300 K), b (T = 370 K) and c (T = 300 K, distance-dependent dielectric constant), respectively, as defined in the Methods section, for both rifamycins S and O. Tables 2, 3 and 4 summarise relative circular statistics. Run d (1000 ps simulation compared to 80 ps for run c) was performed in order to explore low-frequency conformational rearrangements, and the resulting circular statistics for the ansa backbone torsion angles are in Table 5. The distribution is in Figure 5.

An examination of correlations between the variations of torsion angles in the solid state and in molecular dynamics simulations may suggest whether the conformational variety in the solid state mirrors dynamic behaviour. Correlation coefficients were calculated for torsion angles by using circular mean and circular standard deviations, and their significance was evaluated.

For the sample of crystal structures, correlation coefficients between torsion angles were calculated separately for active and non-active compounds. Then the probability that these values were significantly higher than those obtainable from randomly distrib-

Table 1. Circular statistics describing the distributions of the ansa chain torsion angles T1–T17 in crystalline active and non-active rifamycins

	Active crystalline rifamycins			Non-active crystalline rifamycins		
	$\overline{\tau}(i)$	$\overline{r}(i)$	$s_{\mathrm{circ}}(i)$	$\overline{\tau}(i)$	$\overline{r}(i)$	$s_{\mathrm{circ}}(i)$
T1	177.60	0.92	22.26	−170.55	0.60	50.94
T2	74.00	0.61	50.46	39.49	0.39	63.15
T3	3.12	0.97	13.06	−0.74	1.00	4.90
T4	175.99	0.99	9.19	171.50	0.64	48.44
T5	−177.78	1.00	4.89	175.04	0.95	17.47
T6	−45.53	0.92	23.03	68.18	0.09	77.34
T7	179.31	1.00	4.76	−173.70	0.87	28.69
T8	−175.94	1.00	3.56	−174.01	0.88	28.12
T9	58.33	1.00	5.54	91.41	0.77	38.75
T10	−177.60	0.98	10.17	−169.20	0.61	50.63
T11	167.70	0.99	8.48	161.43	0.84	32.48
T12	179.86	0.98	10.21	−171.12	0.56	53.97
T13	−170.91	1.00	4.64	177.43	0.28	68.98
T14	−119.46	0.69	45.35	137.42	0.74	41.34
T15	−176.76	1.00	3.14	−172.40	0.94	20.63
T16	−121.07	0.49	57.62	109.05	0.59	51.80
T17	−63.81	0.99	9.38	−73.80	0.98	11.86

$\overline{\tau}(i)$ (°) is the torsion angle circular mean, $\overline{r}(i)$ and $s_{\mathrm{circ}}(i)$ (°) are the concentration parameter and circular standard deviation, representing the angular dispersion of the sample. Their definition is discussed in the Methods section.

uted uncorrelated points was assessed. Attention was focused on the pairs of variables that were correlated with probability higher than 90%. The matrix of correlation coefficients is represented in Figure 6 as a density plot in which black boxes correspond to probabilities greater than 90%. Figure 6a refers to active molecules and Figure 6b refers to non-active molecules. As expected, active molecules show many more correlations than non-active molecules, because they are required to match the active pattern, while lack of activity can be due to several different reasons. For molecular dynamics simulations, the matrix of correlation coefficients was considered for rifamycin S and rifamycin O, run d. The molecular conformations stored during the simulation are not independent, so the absolute value of correlation coefficients rather than significance levels was used in order to identify the most relevant features of the matrix. For each matrix, the root mean square deviation of the list of correlation coefficients was calculated and used as a threshold for selecting meaningful correlations. About 20% of the values were above the threshold. Figures 6c and d report the resulting matrices for rifamycin S and rifamycin O, respectively. Correlation coefficients above the threshold are marked by black boxes.

Table 2. Circular statistics describing the distributions of the ansa chain torsion angles T1–T17 resulting from molecular dynamics simulations for rifamycin S and rifamycin O, run a

	Rifamycin S			Rifamycin O		
	$\overline{\tau}(i)$	$\overline{r}(i)$	$s_{\mathrm{circ}}(i)$	$\overline{\tau}(i)$	$\overline{r}(i)$	$s_{\mathrm{circ}}(i)$
T1	−177.83	0.99	7.59	−176.22	0.99	7.46
T2	98.57	0.95	18.14	56.63	0.98	9.99
T3	0.33	0.99	5.94	2.88	1.00	5.68
T4	−170.17	0.92	23.08	38.34	0.98	11.21
T5	−179.40	1.00	5.69	179.55	1.00	5.19
T6	−57.48	0.91	23.85	103.40	0.96	16.11
T7	−173.97	0.99	8.89	−173.91	0.98	10.50
T8	−172.89	0.99	8.98	−168.32	0.99	8.65
T9	69.42	0.98	12.11	90.13	0.95	18.08
T10	−170.66	0.99	9.10	−171.88	0.99	7.86
T11	171.29	0.99	7.96	178.31	0.99	7.92
T12	179.31	0.99	8.58	176.32	0.99	8.39
T13	177.15	0.98	10.40	67.69	0.99	8.85
T14	−90.58	0.99	8.48	123.70	0.98	11.59
T15	178.09	1.00	4.93	−179.23	1.00	5.25
T16	−158.27	0.99	9.91	20.68	0.97	13.33
T17	−53.80	0.99	8.06	−67.98	0.99	8.35

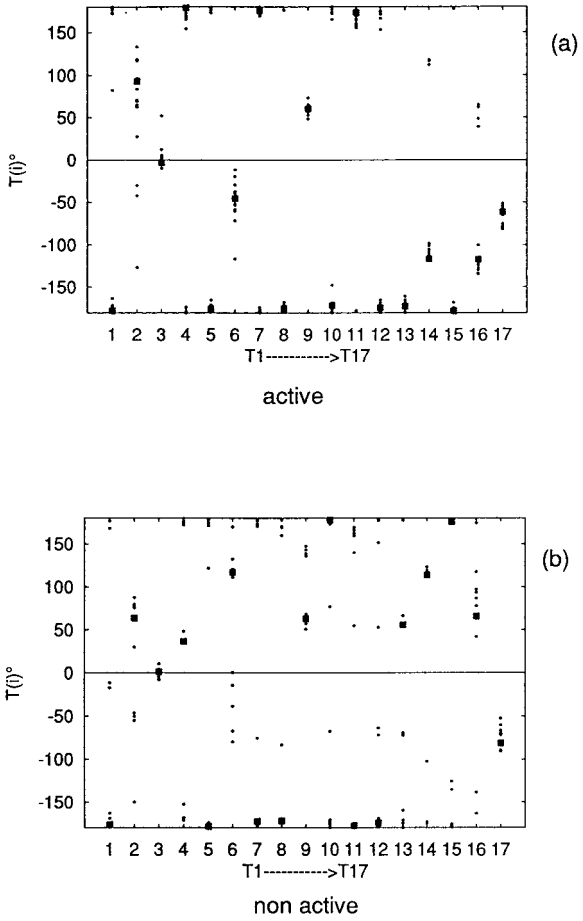

Figure 1. Distributions of the ansa chain torsion angles T1→T17 in rifamycin crystal structures for (a) active and (b) non-active compounds. For the definition of torsion angles, see the text and Scheme 1. Torsion angles relative to rifamycin S (a) and rifamycin O (b) are highlighted by bold squares.

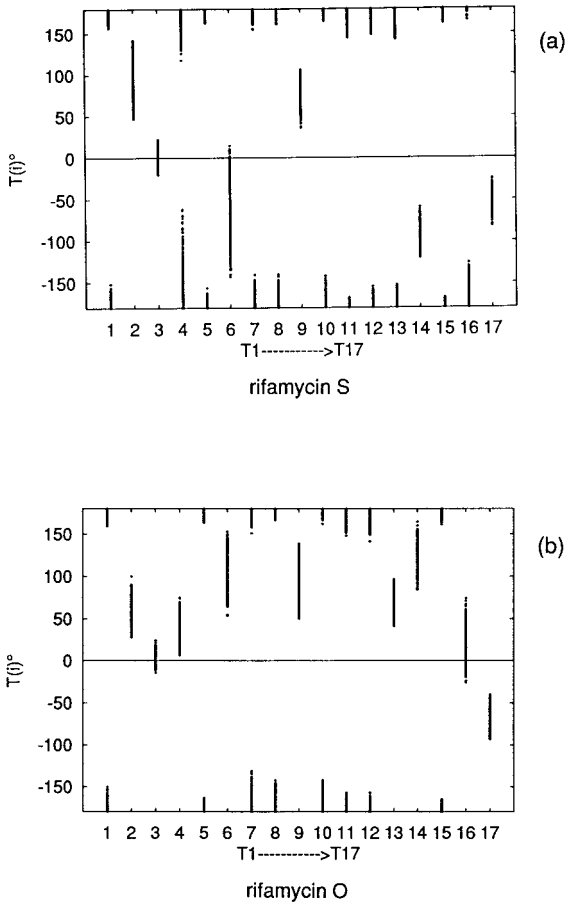

Figure 2. Distribution of the ansa chain torsion angles T1→T17 during molecular dynamics run a for (a) rifamycin S and (b) rifamycin O.

Discussion

From the comparison of the distributions of torsion angles for active and non-active rifamycins (Figure 1, Table 1), some indications can be derived. First of all, torsion angles for active compounds follow a well-defined pattern, while for non-active molecules they are much more scattered, as indicated by the very high values of sample standard deviations. This supports the hypothesis that active rifamycins have at least one common stable conformation in solution, resulting in very similar crystal structures for all active compounds. It must be noted that all crystals of active rifamycins have been obtained from polar solvents and some of them crystallise as solvates. The occurrence of the same molecular conformation in 16 different crystalline environments for active molecules indicates that rifamycin flexibility probably does not produce multiple stable conformers capable of modifying the pharmacophore in polar solvents. The major conformation present in solution is likely to be preserved in crystals. Secondly, the maximum differentiation in conformation of the ansa chain between active and non-active compounds is at C16-C17-C18-C19(T4), C18-C19-C20-C21(T6), C21-C22-C23-C24(T9), C25-C26-C27-C28(T13) and C26-C27-C28-C29(T14). This agrees with the observation that the active pattern for the pharmacophore (O1, O2, O9, O10) can be destroyed by two factors: a rigid rotation of the ansa central segment C20-C26 around T6 and T13, and a local rearrangement of the central segment involving T9 [9].

A further inspection of Figure 1a and Table 1 reveals that for active rifamycins the distribution of

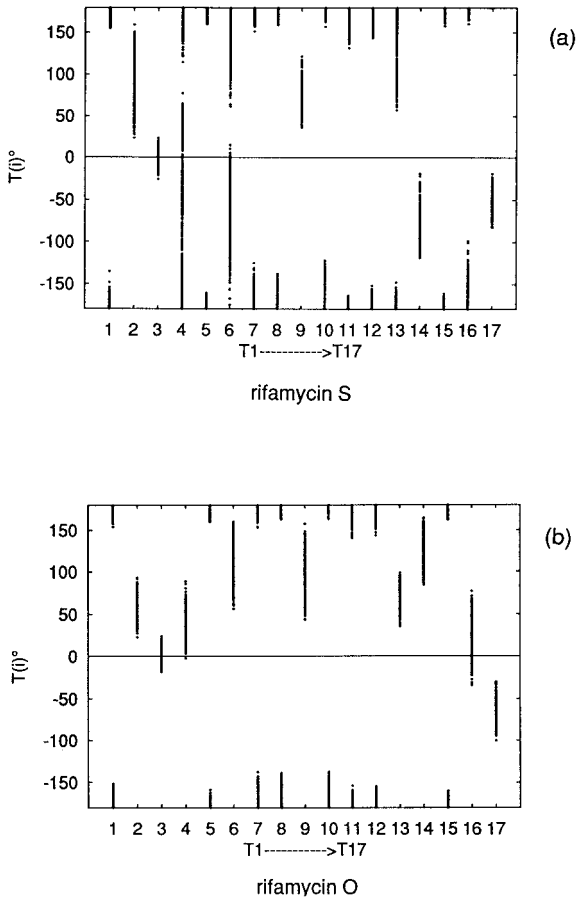

Figure 3. Distribution of the ansa chain torsion angles T1→T17 during molecular dynamics run b for (a) rifamycin S and (b) rifamycin O.

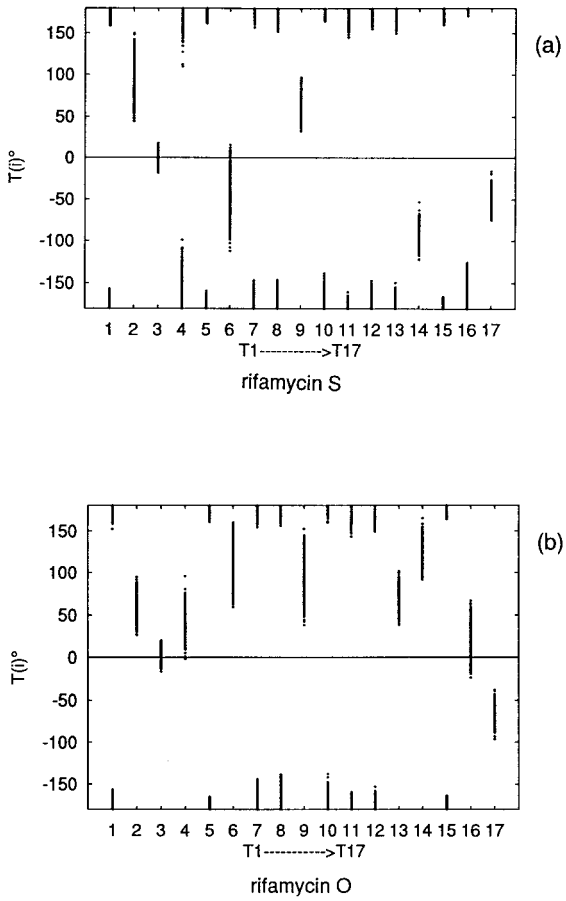

Figure 4. Distribution of the ansa chain torsion angles T1→T17 during molecular dynamics run c for (a) rifamycin S and (b) rifamycin O.

torsion angles T1, T2, T16 at the two junctions between the ansa chain and the pharmacophore is spread, bimodal in the case of T16. If we consider that the different crystal fields expressed in the collection of active rifamycin structures can mimic the intermolecular forces experienced by a rifamycin in solution, the principles of structure correlation [29] relate the distribution of torsions at the junctions to the presence of a shallow minimum in the conformational energy hypersurface (or of low activation energies) in correspondence to the rearrangement of the junctions. This agrees well with the observation of local flexibility and multiple conformations at the junctions in solution by NMR spectroscopy [30]. However, according to the interpretation of spectroscopic data, this mobility does not affect the arrangement of O1, O2, O9 and O10.

With the aim of investigating the possible mechanism of conversion between active and non-active conformations, we have performed molecular dynamics simulations on rifamycin S [20] and rifamycin O [9], chosen as models for active and non-active configurations, respectively. Rifamycin derivatives are usually differentiated by the nature of the substituents at positions 3 and 4 on the chromophore (Scheme 1), which are generally varied in order to tune pharmacokinetic properties. Rifamycin S is active and is the least hindered of all rifamycins, while the conformation found for rifamycin O in the crystal is typical of non-active compounds, even if it is reported among active molecules and the mechanism of action is still controversial. From molecular mechanics studies, it has been suggested that the presence of the bulky substituent in position 4 should prevent a rearrangement leading to active conformation [9]. The choice of rifamycin O as the model for non-active compounds has the aim of elucidating whether the intramolecular steric con-

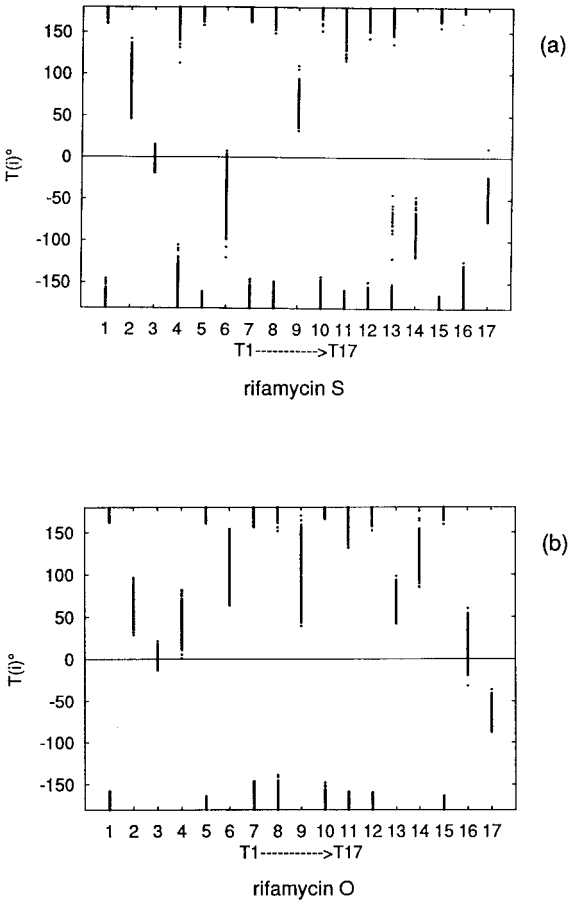

Figure 5. Distribution of the ansa chain torsion angles T1→T17 during molecular dynamics run d for (a) rifamycin S and (b) rifamycin O.

straints determining the solid-state conformation can be overcome by dynamic processes.

The comparison of Tables 2 and 3 shows that augmenting the simulation temperature leads to a significant increase of mobility at T4, T6 and T13 for rifamycin S, as shown by the circular standard deviation which roughly doubles by passing from 300 to 370 K. The dispersion of the other torsion angles is much less affected by increasing the simulation temperature; in particular, the mobility at T1, T2 and T16 appears poorly sensitive to the increase in temperature. This suggests that the energy required for the conformational rearrangements at the junctions is higher than that available in the simulation at 370 K. The increased spread of T4, T6 and T13 with higher temperature can be explained by broad oscillations of the central part of the ansa chain around the hinges at T6 and T13. Rifamycin O is less sensitive to variation in the temperature at which the dynamics is carried out, according to the hypothesis that its structure is sterically constrained. The mean values of torsion angles are quite insensitive to the change in temperature, the largest shifts being for $\overline{\mathrm{T}}4$ and $\overline{\mathrm{T}}6$ in rifamycin S, both of about 10°, less than one half of the associated standard deviation. Table 4 refers to the molecular dynamic simulation carried out with the distance-dependent dielectric function, in order to account for the effects of the solvent. Compared to Table 2, there are no substantial variations in the mean and angular dispersion of the distributions of torsion angles for both rifamycin S and rifamycin O. The most remarkable difference is found for T9 in rifamycin S, with a shift of 10° in the angular mean value, corresponding roughly to one circular standard deviation. This depends on the fact that the modification of the dielectric function affects mostly the parameters related to the intramolecular hydrogen bond O10-H···O9, but it does not produce any significant conformational variation.

On comparing Tables 4 and 5, it is seen that the only relevant feature emerging on a longer time scale is the possibility of a broader oscillation of methyl C34 for rifamycin S, as shown by the comparison of the values of circular standard deviations for T13 in Table 4 (rifamycin S, 80 ps) and Table 5 (rifamycin

Table 3. Circular statistics describing the distributions of the ansa chain torsion angles T1–T17 resulting from molecular dynamics simulations for rifamycin S and rifamycin O, run b

	Rifamycin S			Rifamycin O		
	$\overline{\tau}(i)$	$\overline{r}(i)$	$s_{\mathrm{circ}}(i)$	$\overline{\tau}(i)$	$\overline{r}(i)$	$s_{\mathrm{circ}}(i)$
T1	−178.45	0.99	8.74	−176.48	0.99	7.81
T2	96.73	0.92	23.16	56.61	0.98	10.44
T3	0.10	0.99	6.48	2.63	0.99	6.35
T4	−159.98	0.36	64.96	38.82	0.98	12.28
T5	179.98	0.99	6.41	179.41	0.99	5.85
T6	−70.19	0.33	66.48	104.60	0.95	17.79
T7	−173.38	0.98	10.15	−173.93	0.98	10.29
T8	−171.47	0.98	10.60	−169.01	0.99	9.79
T9	71.21	0.98	12.72	89.14	0.94	19.82
T10	−167.08	0.97	12.94	−171.52	0.99	8.51
T11	167.89	0.98	10.79	177.37	0.99	8.76
T12	177.62	0.98	10.00	176.64	0.99	9.08
T13	170.29	0.91	24.20	68.18	0.99	9.89
T14	−88.39	0.98	12.25	124.14	0.98	12.77
T15	178.27	0.99	5.90	−179.46	0.99	5.88
T16	−158.06	0.98	11.71	20.65	0.96	15.68
T17	−53.52	0.99	9.43	−67.21	0.99	9.53

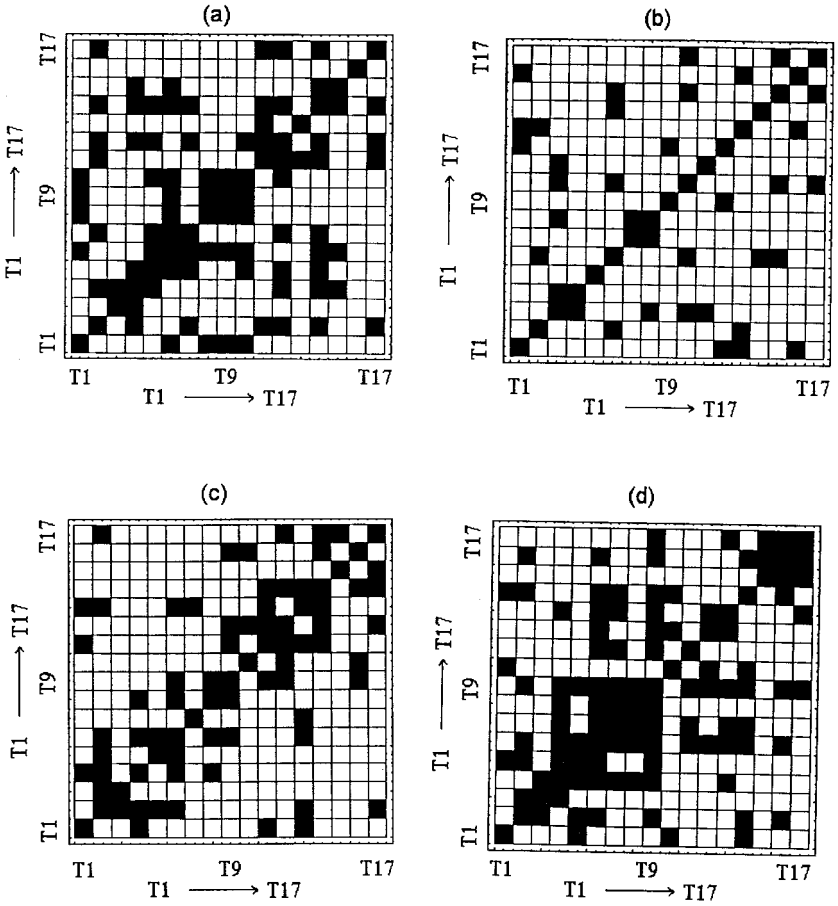

Figure 6. Density plot of the correlation matrix between the 17 ansa chain torsion angles for (a) crystal structures of active compounds, (b) crystal structures of non-active compounds, (c) molecular dynamics simulation of rifamycin S and (d) molecular dynamics simulation of rifamycin O. Significant correlation coefficients are indicated by black boxes.

S, 1000 ps). In the longer simulation, T13 reaches values around −60°, which bring the methyl C34 on the same side as O1 and O2 with respect to the ansa chain, pushing the acetyl group at C25 backwards (see Scheme 1 for the three-dimensional structure of rifamycin S). The arrangement of the four oxygens O1, O2, O9 and O10 is not affected. The relatively high mobility of C34 for the unhindered rifamycin S has been previously suggested [9] based on molecular mechanics calculations. With respect to rifamycin O, the inspection of torsion angles gives evidence of bimodal distributions for T6 and T9. This indicates the presence of a second conformer, which differs from the one found in the crystal (T6, T9 = 90° and 140°, respectively, compared with about 120° and 60° in the crystal). This means that the bond C21-O10 is rotated about the direction C19-C20 and tends to become parallel to the chromophore, while the bond C23-O9 preserves its orientation pointing to the naphthoquinone, due to the hindrance between C34 and the oxolanone substituent (Scheme 1) [9]. Consequently, also the second conformation found for rifamycin O is not comparable to the one typical of active molecules.

Molecular dynamics simulations did not give evidence of a feasible mechanism for conversion from non-active-like to active-like conformation for rifamycin O. The comparison between distributions of torsion angles in the crystal state and those resulting by molecular dynamics simulations is necessarily limited to active compounds, since non-active molecules do not have common features, as evidenced by the scattered pattern of Figure 1b. The analysis of Table 1 shows that the distributions of torsion angles in crystals of active rifamycins reproduce very closely the results of molecular dynamics simulation for rifamycin S in the angular mean values. The only

Table 4. Circular statistics describing the distributions of the ansa chain torsion angles T1–T17 resulting from molecular dynamics simulations for rifamycin S and rifamycin O, run c

	Rifamycin S			Rifamycin O		
	$\overline{\tau}(i)$	$\overline{r}(i)$	$s_{\mathrm{circ}}(i)$	$\overline{\tau}(i)$	$\overline{r}(i)$	$s_{\mathrm{circ}}(i)$
T1	−178.39	0.99	7.10	−176.44	0.99	7.29
T2	97.93	0.96	17.09	57.43	0.98	10.00
T3	0.35	0.99	5.77	2.76	1.00	5.51
T4	−169.27	0.94	19.51	37.54	0.98	11.05
T5	−179.64	1.00	5.69	179.51	1.00	5.31
T6	−46.49	0.94	19.62	106.93	0.95	17.69
T7	−174.99	0.99	8.29	−173.68	0.98	10.48
T8	−179.91	0.98	9.93	−169.63	0.98	10.48
T9	59.29	0.99	9.21	85.07	0.93	20.74
T10	−174.61	0.99	8.23	−171.81	0.99	8.61
T11	174.46	0.99	7.94	177.71	0.99	8.56
T12	−177.15	0.99	8.74	177.72	0.99	9.50
T13	179.35	0.99	9.14	69.36	0.99	9.51
T14	−90.26	0.99	8.15	125.14	0.98	11.09
T15	177.82	1.00	5.02	−178.89	1.00	5.28
T16	−157.29	0.99	9.60	18.87	0.98	12.66
T17	−51.68	0.99	7.86	−66.35	0.99	7.88

Table 5. Circular statistics describing the distributions of the ansa chain torsion angles T1–T17 resulting from molecular dynamics simulations for rifamycin S and rifamycin O, run d

	Rifamycin S			Rifamycin O		
	$\overline{\tau}(i)$	$\overline{r}(i)$	$s_{\mathrm{circ}}(i)$	$\overline{\tau}(i)$	$\overline{r}(i)$	$s_{\mathrm{circ}}(i)$
T1	−178.31	0.99	7.15	−177.09	0.99	7.08
T2	96.88	0.95	17.26	59.42	0.98	10.96
T3	0.27	1.00	5.51	2.83	1.00	5.51
T4	−169.37	0.95	18.65	41.10	0.98	11.59
T5	−179.81	0.99	5.74	179.96	1.00	5.39
T6	−46.92	0.94	19.16	106.02	0.95	17.48
T7	−175.34	0.99	8.77	−178.47	0.98	10.36
T8	−179.00	0.99	9.40	−176.16	0.99	9.17
T9	59.76	0.99	9.71	103.19	0.84	32.58
T10	−174.82	0.99	8.24	−173.70	0.99	7.71
T11	172.42	0.98	10.89	175.25	0.98	11.31
T12	−177.91	0.99	9.35	177.68	0.99	8.37
T13	−179.77	0.96	16.41	67.72	0.99	8.35
T14	−89.54	0.99	8.55	121.92	0.98	12.08
T15	177.87	1.00	5.18	−179.16	1.00	5.35
T16	−157.15	0.99	9.59	16.06	0.97	12.90
T17	−51.44	0.99	8.30	−65.00	0.99	8.2

three relevant differences are for T2, T14 and T16, where multimodal distributions are found in the solid state (Figure 1a), and are not reproduced by dynamics (Figures 2–5). The field of existence of multiple conformers connected to the observed multimodal distributions could be explored by performing molecular dynamics from different starting conformations or by using conformational search procedures. In view of the computational effort required, crystal data contain more easily accessible, albeit possibly partial, information about multiple conformational minima. More relevant discrepancies are found regarding the dispersion of angular data about the mean values. If we consider Table 5 as the reference for dynamic simulations, we observe that the torsion angles at the junctions are more widely dispersed in the solid state than in the simulation, partly due to the above-mentioned multimodality, and partly due to the presence in the crystal sample of molecules with different chemical structure, as in the case of T3 (C16-C17 is a double bond in rifamycin S, but it is a single bond in one active compound [22] and T3 deviates significantly from 0°). Conversely, torsion angles in the central part of the ansa chain have slightly lower angular dispersion in the crystal sample than in dynamic simulations. We might derive the conclusion that in an organised environment like a crystal field, the mobility at the junctions is reproduced by 'freezing' multiple conformers also present in solution, while the less flexible part of the ansa chain is constrained in a rather sharply defined pattern, as required for activity.

The validity of considering the collection of active rifamycin crystal structures as a model for representing the dynamic field of stability of molecular conformations in an organised surrounding such as in solution or in the interaction with DDRP can be further tested by examining the correlations between torsion angles. From Figure 6c, it appears that for the less constrained rifamycin S the correlation of torsional motion is confined to groups of neighbouring atoms, as shown by the clustering of high correlation coefficients near the diagonal. In rifamycin O, it seems that longer range correlations are involved, as shown by the larger spread of high values off the diagonal. This is related to the sterically hindered structure of the molecule, which probably requires more communication between distant fragments of the ansa chain in order to make motion feasible. Although long-range correlations are present in Figure 6a, the matrix obtained from crystal structures is more similar to the one characteristic of rifamycin S than of rifamycin O. In fact, the number of significant correlation coefficients

common to crystals and dynamics divided by the total number of significant correlation coefficients is higher for rifamycin S (13/30) than for rifamycin O (12/46).

Conclusions

The distribution of the ansa chain torsion angles in rifamycin crystals is different for active and non-active molecules. For active compounds, the distribution of torsion angles in the crystals is related to the population of conformers of the molecular ensemble generated during the molecular dynamics simulation. Multiple conformations at the junctions, not accessible in the molecular dynamics runs, are revealed by an inspection of crystal structures. The correlations among torsion angles in the crystal structures are partially related to concerted conformational distortions observed during molecular dynamics simulation. The analysis of molecular dynamics does not give evidence of easy mechanisms for a rearrangement of rifamycin O from the sterically constrained non-active conformation found in the crystal into the active pattern.

References

1. Lancini, G. and Zanichelli, W., In Perlman, D. (Ed.) Structure-Activity Relationship among the Semisynthetic Antibiotics, Academic Press, New York, NY, 1977, pp. 531–600.
2. Brufani, M., Cerrini, S., Fedeli, W. and Vaciago, A., J. Mol. Biol., 87 (1974) 409.
3. Brufani, M., Cellai, L., Cerrini, S., Fedeli, W. and Vaciago, A., Mol. Pharmacol., 14 (1978) 693.
4. Brufani, M., Cellai, L., Cerrini, S., Fedeli, W., Segre, A. and Vaciago, A., Mol. Pharmacol., 21 (1982) 394.
5. Arora, S.K., Mol. Pharmacol., 23 (1983) 133.
6. Arora, S.K. and Main, P., J. Antibiot., 37 (1984) 178.
7. Arora, S.K., J. Med. Chem., 28 (1985) 1099.
8. Bacchi, A., Mori, G., Pelizzi, G., Pelosi, G., Nebuloni, M. and Panzone, G.B., Mol. Pharmacol., 47 (1995) 611.
9. Bacchi, A., Ferrari, P., Nebuloni, M. and Pelizzi, G., J. Med. Chem., 41 (1998) 2319.
10. Bacchi, A. and Mori, G., CC'97: Conferentia Chemiometrica of Hungarian Chemical Society and Hungarian Academy of Sciences, Budapest, 21–23 August 1997.
11. Allen, F.H. and Kennard, O., Chem. Des. Autom. News, 8 (1993) 1 and 31.
12. Gadret, M., Goursolle, M., Leger, J.M. and Colleter, J.C., Acta Crystallogr., B31 (1975) 1454.
13. Arora, S.K., Acta Crystallogr., B37 (1981) 152.
14. Cellai, L., Cerrini, S., Segre, A., Brufani, M., Fedeli, W. and Vaciago, A., J. Chem. Soc., Perkin Trans. 2, (1982) 1633.
15. Brufani, M., Cellai, L., Cerrini, S., Fedeli, W., Marchi, E., Segre, A. and Vaciago, A., J. Antibiot., 37 (1984) 1623.
16. Cellai, L., Cerrini, S., Lamba, D., Brizzi, V. and Brufani, M., J. Chem. Res. (S), (1987) 328.
17. Cerrini, S., Lamba, D., Burla, M.C., Polidori, G. and Nunzi, A., Acta Crystallogr., C44 (1988) 489.
18. Bartolucci, C., Cellai, L., Cerrini, S., Lamba, D., Segre, A., Brizzi, V. and Brufani, M., Helv. Chim. Acta, 73 (1990) 185.
19. Leger, J.M. and Carpy, A., Helv. Chim. Acta, 74 (1991) 326.
20. Arora, S.K. and Arjunan, P., J. Antibiot., 45 (1992) 428.
21. Bartolucci, C., Cellai, L., Cerrini, S., Di Filippo, P. and Lamba, D., Helv. Chim. Acta, 75 (1992) 153.
22. Bartolucci, C., Cellai, L., Cerrini, S., Di Filippo, P., Lamba, D., Segre, A., Bianco, A.D., Guise, M., Pasquali, V. and Brufani, M., Helv. Chim. Acta, 76 (1993) 1459.
23. SYBYL 6.3, Copyright 1991–1996 Tripos Associates Inc., St. Louis, MO, U.S.A.
24. Frisch, M.J., Trucks, G.W., Head-Gordon, M., Gill, P.M.W., Wong, M.W., Foresman, J.B., Johnson, B.G., Schlegel, H.B., Robb, M.A., Replogle, R.S., Gomperts, R., Andres, J.L., Raghavachari, K., Binkley, J.S., Gonzalez, C., Martin, R.L., Fox, D.J., Defrees, D.J., Baker, J., Stewart, J.J.P. and Pople, J.A., Gaussian92 1992, Gaussian Inc., Pittsburgh, PA, U.S.A.
25. Allen, F.H. and Johnson, O., Acta Crystallogr., B47 (1991) 62.
26. Batschelet, E., Circular Statistics in Biology, Academic Press, London, 1981.
27. Mardia, K.V., Statistics of Directional Data, Academic Press, London, 1972.
28. Blessing, R.H., J. Am. Chem. Soc., 105 (1983) 2776.
29. Burgi, H.B. and Dunitz, J.D. (Eds.) Structure Correlation, VCH, Weinheim, 1994.
30. Cellai, L., Cerrini, S., Segre, A., Brufani, M., Fedeli, W. and Vaciago, A., J. Org. Chem., 47 (1982) 2652.